ELSEVIER

Inorganica Chimica Acta 258 (1997) 53–63

Inorganica Chimica Acta

Preparation and characterization of pyridinium-*n*-carboxylate trioxochromate (VI) ($n=3, 4$) and pyridinium-4-carboxylic pyridine-4 carboxylate trioxochromate (VI) hemihydrate

Pedro Martin-Zarza [a], Pedro Gili [a,*], Catalina Ruiz-Perez [b], Fernando V. Rodriguez-Romero [b], German Lotter [c], Juan M. Arrieta [d], Maricel Torrent [e], Jordi Mestres [e], Miquel Solà [e], Miquel Duran [e,*]

[a] *Departamento de Química Inorgánica, Universidad de La Laguna, E-38204 La Laguna, Tenerife, Canary Islands, Spain*
[b] *Departamento de Física Fundamental y Experimental, Universidad de La Laguna, E-38204 La Laguna, Tenerife, Canary Islands, Spain*
[c] *Pharmazeutische Institut der Universität München, D-8000, München 2, Germany*
[d] *Departamento de Química Inorgánica, Universidad del País Vasco, Apdo 644, Bilbao, Spain*
[e] *Departament de Química and Institut de Química Computacional, Universitat de Girona, 17071 Girona, Catalonia, Spain*

Received 9 May 1996; accepted 23 September 1996

Abstract

Three chromium (VI) compounds have been synthesized at room temperature by reaction of CrO_3 with pyridinium carboxylic acids in water. An X-ray diffraction study of pyridinium-3-carboxylate trioxochromate, [3-HNicCrO$_3$] (**1**), indicates crystallization in the triclinic system, space group $P\bar{1}$ (No. 2) with $Z=2$ and lattice parameters $a=7.548(3)$ Å, $b=6.593(3)$ Å, $c=7.820(3)$ Å, $\alpha=90.01(2)°$, $\beta=91.65(2)°$, $\gamma=89.91(2)°$ and $V=389.0(3)$ Å^3 at 25(2)°C. The chromium atom presents a distorted tetrahedral coordination, with the three Cr–O (terminal oxygen) bond lengths ranging from 1.588(6) Å to 1.603(6) Å, and the fourth Cr–O bond being 1.881(4) Å long. The symmetry is C_s, all atoms lying in the same plane with the exception of two terminal oxygens. 3-HNicCrO$_3$ molecules interact by hydrogen bonds. This experimental work has been complemented with a theoretical study to discuss geometries, relative energies for the two possible isomers of compound **1**, IR and UV–visible spectroscopic data, and electronic analyses. Powder data for pyridinium-4-carboxylic pyridine-4-carboxylate trioxochromate hemihydrate, [4-HNic][4-NicCrO$_3$] (**2**), and pyridinium-4-carboxylate trioxochromate, [4-HNicCrO$_3$] (**3**), are also reported.

Keywords: Crystal structures; Chromium complexes; Oxide complexes; Pyridinium carboxylic acids complexes

1. Introduction

The preparation of dichromates of organic bases has drawn special interest because these compounds can be used either as reagents in selective oxidation processes of organic substrates, or as intermediates in the synthesis of new species of chromium in lower oxidation states [1–4]. As it has been recently reported [5,6], when CrO_3 reacts with organic bases dichromates and trichromates of organic cations are obtained, whereas the intimate behaviour of the CrO_3 system in front of organic acids remains still quite unknown.

Although oxidations by chromium (VI) have been widely explored since the very beginning of organic chemistry, the topic is of current concern, as exemplified by the extensive number of papers in which at least one step involves the use of an oxochromium (VI) reagent [4,7]. Unfortunately, the chromic byproduct residues are usually poisonous. Chromium (VI) toxicity and mutagenicity has been the subject of a recent review [8]. Hexavalent chromium compounds have long been recognized to cause genotoxic effects in all kinds of intact cells and animal systems, and, more important, cancer in humans [9–12]. A detailed characterization of a series of complexes obtained from the reduction of chromium (VI) with ascorbic acid, cysteine and glutathione has been reported by Cieslak-Golonka and Raczko [13]. Another chromium (VI) complex, with sulphur instead of oxygen, has been studied by Brauer and Wetterhahn [14], who have provided structural evidence for a chromium (VI)–glutathione (GS) thioester. Meloni and Czernuszewicz [15] have confirmed the previously proposed $GSCrO_3^-$ structure [14] in which

* Corresponding authors.

PII S0020-1693(96)05512-0

the cysteinyl thiolate of glutathione is bound to Cr(VI). These species belong to a group of chromium (VI) compounds that have revealed some mutagenic activities, as shown by the reduction of the chromium (VI) ion with important redox-active cellular components of low molecular weight, e.g. ascorbic acid, glutathione or cysteine [13,16,17].

However, little attention has been paid to the synthesis of new compounds containing Cr(VI) based on other acids of low molecular weight which are also involved in the process of chromium (VI) metabolism, e.g. nicotinic and isonicotinic acids. Interestingly, the last two acids are both hydrosoluble and resistant to the oxidation by CrO_3, leading to Cr(VI) compounds of low solubility in presence of CrO_3. Hence, considering environmental purposes, these complexes could be potentially used in the elimination of toxic chromium residues.

In particular, the nicotinic acid is an important water-soluble vitamin with a well-known biological role [18]. It has been shown to be involved in a variant of the pyridine–Cr(VI) family of oxidizing agents as reported by López et al. [19]. This chromium (VI) compound, derived from nicotinic acid and chromium trioxide, was first described as nicotinic acid dichromate (NDC) [19]. Matikainen et al. [20] showed later that NDC is, in fact, a mixed chromic/carboxylic anhydride betaine instead of a dichromate salt as originally assumed [19], several misconceptions having still to be clarified. No similar previous studies exist yet on isonicotinic-based Cr(VI) oxidants.

We consider thus in this paper the compounds formed between hydrated CrO_3 and the pyridinium-*n*-carboxylic acids, where $n=3,4$ corresponds to nicotinic (niacin) and isonicotinic acids, respectively. In particular, an X-ray analysis of pyridinium-3-carboxylate trioxochromate (VI), [3-$HNicCrO_3$] (**1**) is reported, this species being a new crystal phase of the compound already described by Matikainen et al. [20]. We have carried out the synthesis of compound **1** under conditions differing from the original directions described by López et al. [19]. From our study, this compound can be considered to be a pyridinium derived organic ligand and a chromate as part of the same molecule, interacting as an ion pair complex. Besides compound **1**, we also report the synthesis of pyridinium-4-carboxylic-pyridine-4-carboxylate trioxochromate (VI) hemihydrate, [4-HNic][4-$NicCrO_3$]·$0.5H_2O$ (**2**), and pyridinium-4-carboxylate trioxochromate(VI), [4-$HNicCrO_3$] (**3**) which, to our knowledge, have been prepared and characterized for the first time. An understanding of the structures of these complexes may be quite useful in rationalizing their properties, usefulness and functionality (or lack thereof).

The experimental study is complemented by a theoretical analysis. It is clear that nowadays computational methods provide a valuable complementary tool in the structural characterization of inorganic compounds. From a theoretical point of view, the last few years have seen a growing number of applications of quantum-mechanical methods to inorganic and organometallic structural and spectroscopic determinations [21,22]. In particular, $Cr(CO)_6$, as well as other related compounds [23–28], has been well characterized and the nature of its bonding discussed in depth by means of computational methods, the chromium (VI) species deserving special emphasis [29–31]. The outcome of this presently large amount of theoretical studies is that quantum chemistry has reached a stage where at least semiquantitative structural and spectroscopic determinations can be made [32,33], thus becoming a helpful support for experimental results.

The aim of the present paper is thus twofold; the first purpose is to present the synthesis of three compounds, along with their chemical analysis, IR, UV–vis and ^1H NMR characterization, and the structural determination by single-crystal X-ray diffraction of pyridinium-3-carboxylate trioxochromate (VI). A second goal of this investigation is to carry out an ab initio theoretical study in order to discuss and complement the results obtained experimentally. In the next two sections, the experimental methods will be described first, whereas the computational techniques used to actually carry out calculations will be presented later. Finally, a discussion of both experimental and theoretical results will be offered.

2. Experimental

2.1. Preparation of compounds

2.1.1. Preparation of pyridinium-3-carboxylate trioxochromate (VI), [3-$HNicCrO_3$] (1)

A solution of CrO_3 (2 g, 20 mmol) in 20 ml of H_2O was mixed with another solution containing pyridine-3-carboxylic acid (2.46 g, 20 mmol) in 50 ml of water at room temperature. Water was added to solution until the total volume was 100 ml. An orange polycrystalline solid was deposited after keeping the solution for 1 week at room temperature. The solid product was recrystallized from solution of CrO_3 (4.92 g, 40 mmol) in 100 ml of H_2O. Well-formed prismatic orange crystals suitable for X-ray diffraction studies were obtained. *Anal.* Calc. for $CrC_6H_5NO_5$: C, 32.30; H, 2.26; N, 6.28. Found: C, 32.18; H, 2.19; N, 6.12%.

2.1.2. Preparation of pyridinium-4-carboxylic-pyridine-4-carboxylate trioxochromate(VI) hemihydrate, [4-HNic][4-$NicCrO_3$]·$0.5H_2O$ (2)

This needle shaped orange compound was prepared as described above for **1**, except that it was not recrystallized from a solution of CrO_3. *Anal.* Calc. for $CrC_{12}H_{10}N_2O_7 \cdot 0.5H_2O$: C, 40.57; H, 3.12; N, 7.89. Found: C, 40.60; H, 3.10; N, 7.83%.

2.1.3. Preparation of pyridinium-4-carboxylate trioxochromate(VI), [4-HNicCrO$_3$] (3)

When the mother liquor containing **2** was kept for few weeks at room temperature, orange crystals of **3** were obtained. *Anal.* Calc. for $CrC_6H_5NO_5$: C, 32.30; H, 2.26; N, 6.28. Found: C, 32.21; H, 2.18; N, 6.00%.

All reagents commercially obtained were of reagent grade.

2.2. Spectroscopic equipment and elemental analyses

Infrared spectra were recorded in the range 4000–250 cm^{-1} on a Nicolet 710 FT spectrophotometer using KBr pellets. Solid-state electronic spectra were run on a Perkin-Elmer 550S spectrophotometer after dilution of the sample in $BaSO_4$, in the 200–900 nm spectral range. ^{1}H NMR spectra were recorded at 297 K on a Bruker AC 200 spectrometer at 200 MHz, with tetramethylsilane as internal standard after dilution of the sample in deuterated DMSO. Elemental analyses were performed with a Carlo Erba 1106 automatic analyser.

2.3. X-ray crystallographic measurements of [3-HNicCrO$_3$]

Crystallographic data appear in Table 1. Crystals suitable for X-ray diffraction studies were grown directly from the aqueous reaction mixture. A prismatic orange crystal of approximate dimensions 1.00×0.22×0.30 mm was mounted as proteine crystal on a Siemens R3M/diffractometer using balanced filters monochromated Cu Kα radiation. Reflection intensities were standardized to allow for crystal degradation

Table 1
Crystallographic data for [3-HNicCrO$_3$] (1)

Chemical formula	$CrC_6H_5NO_5$
Temperature (°C)	25(2)
fw	223.104
a (Å)	7.548(3)
b (Å)	6.593(3)
c (Å)	7.820(3)
α (°)	90.01(2)
β (°)	91.65(2)
γ (°)	89.91(2)
V (Å^3)	389.0(3)
Space group	$P\bar{1}$ (No. 2)
Z	2
ρ_{calcd} (g cm^{-3})	1.90
Radiation	Cu Kα (1.5418 Å)
F(000)	224
μ(Cu Kα) (mm^{-1})	12.15
2θ range (°)	0.0–114.0
Scan type	variable 8.00–29.50° min^{-1} in ω
Scan speed	ω
Scan range (ω) (°)	2.00
Final *R*(*F*) [a]	0.072
WR(*F*) [b]	0.083
S (goodness of fit)	0.927

[a] $R=(\Sigma\|\|F_o\|-\|F_c\|\|)/\Sigma|F_o|$.
[b] $W=1/[\sigma^2(F)+0.014127F^2]$.

Table 2
Positional parameters and their estimated deviations for [3-HNicCrO$_3$] (1)

Atom	*x*/*a*	*y*/*b*	*z*/*c*	B_{eq} (Å^2)
Cr(1)	0.7014(1)	0.2501(2)	1.0062(1)	4.34(4)
O(1)	0.6556(7)	0.2524(9)	1.2032(6)	6.30(17)
O(2)	0.8096(8)	0.4477(10)	0.9516(7)	6.71(16)
O(3)	0.8087(8)	0.0542(9)	0.9514(7)	6.61(16)
O(4)	0.4848(5)	0.2509(7)	0.8812(5)	4.64(12)
C(1)	0.4882(8)	0.2537(9)	0.7182(8)	3.94(15)
O(5)	0.6229(6)	0.2511(9)	0.6328(6)	5.34(13)
C(2)	0.3106(8)	0.2507(9)	0.6291(8)	3.61(15)
C(3)	0.1569(8)	0.2520(9)	0.7218(8)	3.81(16)
N(1)	0.0001(7)	0.2524(8)	0.6414(7)	4.28(15)
C(4)	0.0201(9)	0.2524(9)	0.4720(8)	3.95(15)
C(5)	0.1274(10)	0.2524(11)	0.3719(8)	4.38(19)
C(6)	0.2955(7)	0.2526(8)	0.4524(8)	3.76(16)

$B_{eq}=(8/3\pi^2)\Sigma a_i^* a_j^* a_i a_j U_{ij}$.

with 2 standard reflections collected every 80 reflections. No significant degradation was observed. Lattice parameters were obtained from 12 reflections in the range $7° \leq 2\theta \leq 25°$. Background measurement was made in the stationary crystal and stationary counter at the beginning and the end of scan, each 50% of total scan time. The cell parameters and the non-existence of systematic absences showed the crystal to belong to a triclinic system, the space group being $P\bar{1}$. A total of 2089 reflections (ω–2θ scan, $2\theta<114°$, $h=\pm8$, $k=\pm7$, $l=+8$) were measured of which 1046 were unique and 907 were considered as observed ($F>4\sigma(F)$). Lorentz, polarization and absorption corrections were applied. The structure was solved by direct methods and refinement made by full-matrix least-squares using the program SHEXTL-PLUS [34]. Hydrogen atoms were located in a difference Fourier map and introduced in the refinement with isotropic thermal parameters. All non-hydrogen atoms were refined with anisotropic thermal parameters. With constrained hydrogen atoms, refinement of all 138 parameters reached convergence with a final parameter mean shift per $\Delta/\sigma=0.027$; maximum and minimum electron density in final difference synthesis was 0.3 and -0.5 e Å^{-3}, respectively. Minimization of the weighted residual R_w led to final discrepancy indices of $\omega R(F)=0.083$ and $R(F)=0.072$. Atomic scattering factors were taken from Ref. [35]. Positional parameters and equivalent isotropic thermal parameters are listed in Table 2. Table 3 gives pertinent bond distances, angles and planes.

2.4. X-ray diffraction in powder

For all compounds the X-ray powder measurements were obtained using a STOE (mod. Stadip) diffractometer, with the sample introduced in a capillary of 0.5 mm of diameter, Cu Kα_1 $\lambda=1.54056$ Å radiation monochromator of germanium, intensity 25 mA and 40 kW, Debye geometry, detector PSD (position sensitive detector), with automatic X-ray recording. Peak intensities were measured as height above the baseline and expressed as a percentage of the strongest

Table 3
Selected lengths, angles and planes for [3-HNicCrO$_3$] (**1**)

Cr(1)–O(1)	1.589(5)
Cr(1)–O(2)	1.603(6)
Cr(1)–O(3)	1.588(6)
Cr(1)–O(4)	1.881(4)
O(4)–C(1)	1.275(8)
C(1)–O(5)	1.233(8)
C(1)–C(2)	1.493(8)
C(2)–C(3)	1.386(8)
C(2)–C(6)	1.383(9)
C(3)–N(1)	1.324(8)
N(1)–C(4)	1.329(8)
C(4)–C(5)	1.380(10)
C(5)–C(6)	1.400(9)
O(3)–Cr(1)–O(4)	107.7(3)
O(2)–Cr(1)–O(4)	107.6(3)
O(2)–Cr(1)–O(3)	108.7(3)
O(1)–Cr(1)–O(4)	107.1(2)
O(1)–Cr(1)–O(3)	113.3(3)
O(1)–Cr(1)–O(2)	112.2(3)
Cr(1)–O(4)–C(1)	118.5(4)
O(4)–C(1)–C(2)	115.0(5)
O(4)–C(1)–O(5)	125.6(6)
O(5)–C(1)–C(2)	119.4(6)
C(1)–C(2)–C(6)	120.9(5)
C(1)–C(2)–C(3)	120.6(5)
C(3)–C(2)–C(6)	118.4(5)
C(2)–C(3)–N(1)	120.1(5)
C(3)–N(1)–C(4)	123.2(5)
N(1)–C(4)–C(5)	119.6(6)
C(4)–C(5)–C(6)	118.7(6)
C(2)–C(6)–C(5)	119.8(6)

Deviations from least-squares plane in Å for all atoms: C(1) (−0.02), C(2) (0.01), C(3) (0.00), C(4) (0.00), C(5) (0.00), C(6) (−0.00), N(1) (0.00), O(4) (0.00), O(5) (0.00), Cr(1) (0.00), O(1) (−0.01), O(2) (−1.30), O(3) (1.29).

Table 4
X-ray powder data for [4-HNic][4-NicCrO$_3$] 0.50 (**2**) and [4-HNicCrO$_3$] (**3**)

(**2**)		(**3**)	
d_{obs}	I_{rel} [a]	d_{obs}	I_{rel} [a]
12.279	25.9	13.741	10.6
5.391	31.2	6.872	42.0
4.756	39.4	6.466	49.1
4.694	100.0	4.257	95.1
4.597	27.8	4.029	49.5
4.386	10.2	3.670	38.9
3.675	14.0	3.398	100.0
3.376	36.5	3.246	36.1
3.293	56.6		

[a] $100I/I_{max}$.

line. For compound **1**, experimental diffraction data were in good accordance with the diffraction pattern calculated on the basis of LAZY-PULVERIX [36] simulation, using the single-crystal parameters described in Table 1. Powder data for **2** and **3** are reported in Table 4.

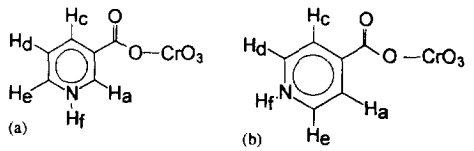

Fig. 1. Hydrogen atom labelled structures: (a) compound **1**; (b) compounds **2** and **3**.

2.5. ^1H NMR spectroscopy

The ^{1}H NMR spectrum of **1** shows peaks at δ 9.09 (singlet), 8.81 (doublet), 8.29 (doublet) and 7.57 (multiplet) ppm, corresponding to H^a, H^e, H^c and H^d resonances, respectively. One broad resonance at δ 3.32 ppm is attributed to H^f of the pyridinium group (Fig. 1(a)).

Compound **2** presents two quadruplets at δ 8.80 and 7.84 ppm, which are assigned to H^e and H^a (Fig. 1(b)). Similarly to the previous compound, one broad resonance at δ 3.66 ppm is attributed to H^f of the pyridinium ring.

Compound **3** presents resonances at δ 9.08 (quadruplet), 8.80 (two doublets), 8.28 (two doublets) and 7.56 (multiplet) ppm, which are assigned to H^a, H^e, H^c and H^d, respectively [37] (Fig. 1(b)).

3. Theoretical

Only one out of the three species considered in this paper has been studied computationally. It is expected that results from a careful study of the 3-HNicCrO$_3$ salt will serve as a model to characterize the main structural and spectroscopic features of these three chromium (VI) compounds. An obvious advantage of choosing the study of **1** instead of **2** emerges from the reduction in computational effort. Furthermore, there is an additional interest due to the possible existence of more than one isomer for **1**, as opposed to the symmetric species **3**, what allows for a richer discussion involving relative energies and thermal aspects.

3.1. Computational details

Energy calculations have been carried out using an ab initio molecular orbital method at the closed-shell SCF level of theory. The large size of the system considered herein and the need to optimize geometries and compute vibrational frequencies prevents use of traditional post-Hartree–Fock optimized correlated wavefunctions. Nevertheless, the effect of the correlation energy has been assessed by means of the computationally less expensive density functional theory. Non-local corrections to the exchange and correlation energies have been incorporated through the forms proposed by Becke [38] and Perdew [39] (BP).

Earlier ab initio studies on inorganic compounds have revealed that a correct choice of the basis set is quite important [40–42]. The present study has used Hehre's extended basis set 3-21G [43] supplemented by a d-function on Cr, and a

polarization function for N and O atoms (exponents being 0.0972944, 0.8 and 0.8, respectively), termed 3-21G*. This basis set has proved to yield reasonably good geometrical results for other chromium (VI) compounds [44].

Full geometry optimizations have always been carried out using Schlegel's method [45]. Transition states have been characterized through the correct number of negative eigenvalues. The infrared spectrum has been computed using the doubly harmonic approximation. Frequencies and normal modes have been analytically calculated through diagonalization of the mass-weighted matrix of energy second derivatives. In turn, line intensities have been made proportional to the square of the derivative of the molecular dipole moment with respect to the respective normal mode. (The whole set of frequencies and intensities is available from the authors upon request.) Electronic spectra have been calculated within approximate density functional theory (Becke-Perdew/3-21G*) through the sum method developed by Ziegler et al. [46]. Calculations mentioned in this paper have been carried out by means of the Gaussian 92/DFT program [47] with the only exception of DFT-based computations of singlet excitation energies, where the Amsterdam Density Functional (ADF) program [48] has been used instead. In this case, STO basis sets of double-ζ quality for C and H, extended with a polarization function for N and O atoms have been used. A triple-ζ set for the 3d shells of chromium has been added in order to be comparable with the 3-21G* Gaussian basis set. The level of frozen core approximation [49] has been 2p for the transition metal and 1s for lighter elements.

The surrounding medium effects have been studied using the Polarized Continuum Medium [50] as implemented in the Gaussian 94 program. Single-point energies for the solvated systems ($\epsilon = 78.36$) have been performed on the geometries previously optimized at RHF level [1].

The analysis of the electron density distribution and its Laplacian, together with the location and characterization of bond critical points, has been performed using the Electra program [51].

4. Results and discussion

Both experimental and theoretical results are presented in this section, which in turn is divided into four subsections. First, structural and energetic analyses are offered, special emphasis being laid on compound **1**. In the second part, the electronic analysis of **1** is dealt with, while infrared and electronic spectra constitute the main goal of the third and last subsections, respectively.

Compounds **1** (and **3**) can be discussed attending to the role of the $HCrO_4^-$ species. Thus, the formation of compound **1** is not performed in a single direct step. As this reaction is carried out in aqueous medium, the CrO_3 forms first the chromate acid anion ($HCrO_4^-$), which is then attacked by the nucleophile $C_5H_4NHCO_2H$ in a second step, finally yielding the desired product ($C_5H_4NHCO_2CrO_3$):

$$CrO_3 + H_2O \rightleftarrows HCrO_4^- + H^+$$

$$C_5H_4NCO_2H + HCrO_4^- \rightarrow C_5H_4NHCO_2CrO_3 + OH^-$$

There is enough evidence [14,52] to think that $HCrO_4^-$ constitutes the key intermediate in this process. Several features about the mechanism may be elucidated studying the central role of $HCrO_4^-$. Moreover, structural and spectroscopic quantum-mechanical analyses of the simple $HCrO_4^-$ anion reveal interesting properties related to the 18-atom product, allowing for a considerable reduction in CPU time. Ab initio theoretical RHF/3-21G* calculations on $HCrO_4^-$ provide at least two features which strongly support the aforementioned attack on $HCrO_4^-$. The first feature is structural: the chromium–oxygen distance in the Cr–O–H group (1.794 Å) is longer than the average chromium–terminal oxygen distance (1.537 Å), providing a hint for a weakness of the metal–oxygen bond [53]. The second feature emerges from the spectroscopic analysis: the –OH fragment acts as an excellent leaving group, as revealed by the intense normal mode corresponding to the stretching ν(Cr–OH) that appears at 734.9 cm^{-1}. Thus, these two features indicate that the –OH group of the $HCrO_4^-$ species can be easily substituted by anions or other groups [52,54]. In our particular case, the –OH group is substituted by the oxygen atom of the carboxylic group of nicotinic acid, the acid proton migrating towards the pyridine nitrogen atom. We do not expect indeed that the two characteristics observed for the gas-phase $HCrO_4^-$ species can be significatively changed in water solution.

4.1. Structural and energetic analyses

Previously reported syntheses [19,20] of compound **1** were performed at 0–5°C and using acetone. Our experimental work conditions were different; we prepared all three compounds at room temperature (ca. 20°C) and no acetone. Besides, we recrystallized **1** in the presence of CrO_3, while in the work of Matikainen et al. [20] it was done in a CrO_3-free medium. These conditions led to a new crystal phase for compound **1**. The non-existence of systematic absences shows the system to be triclinic system. From the analysis of the normalized structural factors, the spatial group is found to be centrosymmetric, $P\bar{1}$.

Fig. 2 shows the experimentally obtained molecular structure of **1**. For the sake of clarity, Cr(1)–O(1), Cr(1)–O(2) and Cr(1)–O(3) distances are referred as an average Cr–O(T) distance, where O(T) stands for terminal oxygen atoms. The chromium presents a distorted tetrahedral coordination, with the three Cr–O(T) bond lengths lying in a 1.588(6)–1.603(6) Å range of values, and the fourth Cr(1)–O(4) being of 1.881(4) Å. Our results are in good agreement with those previously reported by Matikainen et al. [20],

[1] The sphere radii used for atoms were: H, 1.20 Å; C, 1.50 Å; N, 1.50 Å; O, 1.40 Å; and Cr, 0.66 Å. The surrounding medium effect calculations were carried out at 298.15 K.

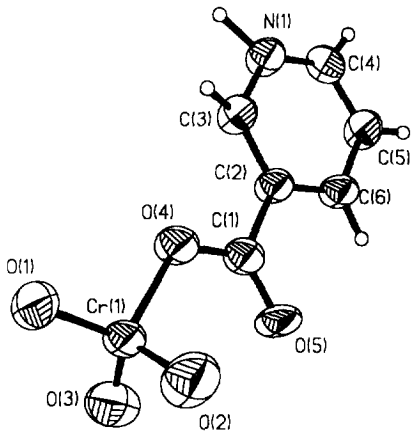

Fig. 2. Molecular structure of compound 3-HNicCrO$_3$ obtained experimentally.

who found an average Cr–O(T) bond distance of 1.592(2)–1.597(2) Å and a Cr(1)–O(4) bond length of 1.869(2) Å. The Cr–O(T) distances found in the literature for Cr–O in mono- and polychromates [55] where the oxygen atoms are nonbridging, are in the range 1.56–1.72 Å, while the Cr–O distances for bridging oxygen atoms are in the interval 1.75–1.86 Å. The value found for Cr(1)–O(4) suggests a weakness of this bond as has been discussed above for the $HCrO_4^-$ anion. Atoms O(1), Cr, O(4) and C(1) are nearly coplanar (dihedral angle, 179.3(3)°). The value for the C(1)–O(5) distance (1.233(8) Å in our work and 1.208(4) Å in the work of Matikainen et al. [20]) is shorter than for C(1)–O(4) (1.275(8) Å here, and 1.294(4) Å in the previous work). Both distances are similar to those found in carboxylate groups, the latter indicating again a weakness of the C–O bond. The C(1)–C(2) bond length (1.493(8) Å in our work, and 1.495(4) Å in that of Matikainen et al. [20]) indicates mainly a character of single bond; thus the possibility of turning through the C(1)–C(2) gives rise to the existence of conformers. In solid phase at room temperature, only the conformer where the O(5) is in *anti* position with respect to nitrogen atom has been observed.

The crystal structure of **1** is shown in Fig. 3, where the 3-HNicCrO$_3$ molecules interact by hydrogen bonds. There are hydrogen bonds between the N–H of the pyridinium and the O(2) and O(5), N(1)–H(1N)···O(2) (2.02(7) Å, 164(5)°) and N(1)–H(1N)···O(5) (2.57(8) Å, 92(4)°), being bifurcated bonds in H(1N).

The optimized structures at the RHF/3-21G* level of theory for the two different 3-HNicCrO$_3$ conformers have been depicted in Fig. 4. Although several starting points in the search procedure have been tried, the energetic minimum has always been located in a C_s-symmetry structure (all atoms lying in the same plane with the exception of the two terminal oxygens), in agreement with experimental structural data (Table 3). The main geometrical parameters of conformer labelled A, together with DFT/3-21G* computed geometry and the observed data, are collected in Table 5, which shows a fairly good agreement between DFT-calculated and experimental bond lengths, whereas SCF bond distances have a larger error. This last point indicates that, in these systems, energy correlation effects are important. As noticed earlier for dichromate [44], Cr–O(T) bond lengths (1.53 Å) are clearly shorter than that for Cr(1)–O(4) (1.90 Å), both distances being comparable to those previously found for $HCrO_4^-$ (1.54 and 1.79 Å, respectively).

When results from Table 3 are compared with earlier experimental data [20], the main bond angles are remarkably

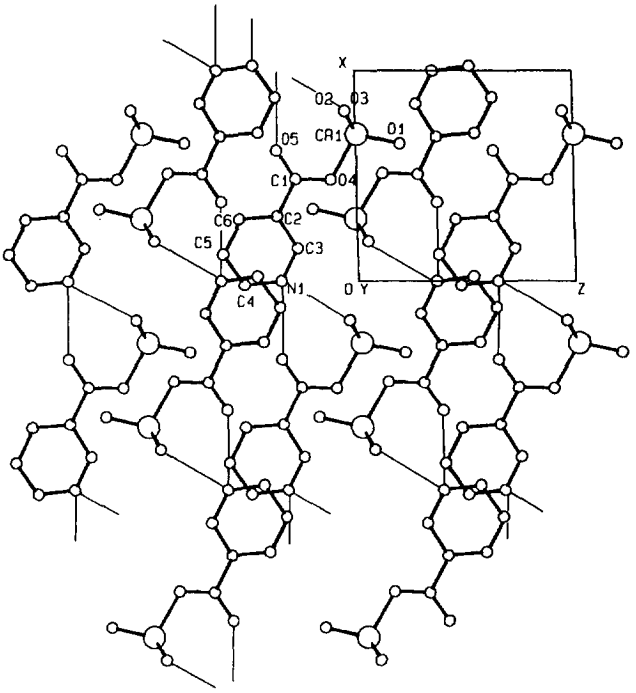

Fig. 3. Crystal structure of 3-HNicCrO$_3$ obtained by X-ray diffraction.

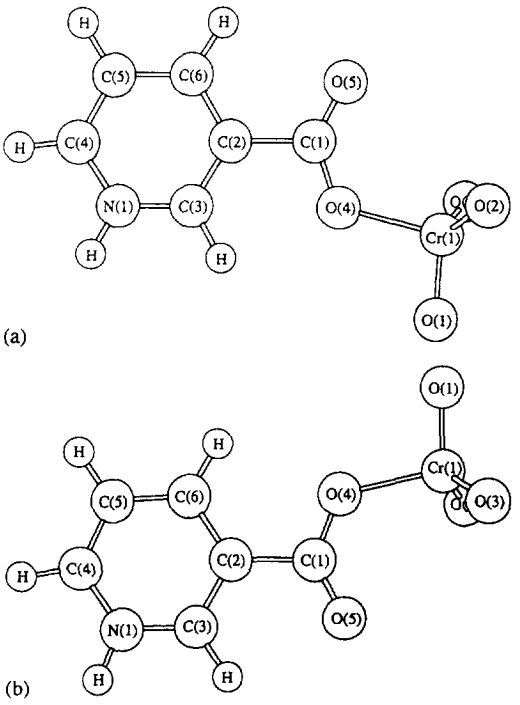

Fig. 4. Optimized structures for the two possible conformers of 3-HNicCrO$_3$ species: (a) conformer A; (b) conformer B.

Table 5
Experimental and optimized geometries (in Å and °) for the 3-HNicCrO$_3$ species, where O(T) stands for terminal oxygens

Geometrical parameters	Calculated		Experimental (conformer A)
	RHF	DFT	
Bond lengths			
Cr(1)–O(T)	1.529	1.599	1.60
Cr(1)–O(4)	1.900	1.894	1.88
C(1)–O(4)	1.281	1.318	1.28
C(1)–O(5)	1.194	1.227	1.23
C(1)–C(2)	1.528	1.516	1.49
C(2)–C(3)	1.371	1.403	1.39
C(3)–N(1)	1.338	1.347	1.32
C(4)–N(1)	1.347	1.344	1.33
C(4)–C(5)	1.366	1.402	1.38
C(5)–C(6)	1.393	1.396	1.40
C(6)–C(2)	1.378	1.401	1.38
Bond angles			
Cr(1)–O(4)–C(1)	125.20	119.40	118.4
C(2)–C(1)–O(4)	110.16	112.11	115.0
O(5)–C(1)–O(4)	132.05	128.09	125.6
O(5)–C(1)–C(2)	117.79	119.79	119.4

well reproduced. Thus, the Cr(1)–O(4)–C(1) and O(5)–C(1)–C(4) were found to be 118.3(2) and 125.3(3)°, respectively [20]. Slightly larger deviations are found for C(2)–C(1)–O(4) or O(5)–C(1)–C(2) bond angles of Table 3, which were reported [20] to be 113.9(3) and 120.9(3)°, respectively, small differences accounting for different crystal phases (a monoclinic system in Ref. [20], but a triclinic system in the present paper). On the other hand, calculated bond angles are not very good at the present RHF level of theory, while a better agreement is encountered at DFT level. To determine the confidence levels for geometrical parameters, and also for relative energies, see Ref. [56], which contains several comparisons of chromium species characterized at 3-21G*/RHF and /DFT levels of theory. Although difficulties in reproducing these bond angles can be still due to basis set incompleteness, it has to be kept in mind that while calculated bond angles come from the consideration of a single isolated molecule in the gas phase, experimental bond angles were extracted from a crystal packed ensemble of molecules. Thus, as shown before [44], it seems that bond angles are very sensitive to the effects of the environment; in this sense, comparisons between calculations and condensed-phase experiments must be always done with some care.

Judging from bond angles and lengths, conformers A and B are nearly identical. However, the structure where the carbonylic oxygen and nitrogen atom adopt an *anti* position (conformer A) is preferred. From relative energies computed for *syn* and *anti* conformers, A and B should be regarded as energetically equivalent. At RHF level the energy difference is only 0.70 kcal mol^{-1}, conformer A being slightly more stable than conformer B. An even smaller difference (0.25 kcal mol^{-1}) is found when energy correlation is taken into account through DFT computations including non-local corrections (BP). These values do not allow us to determine how easily interchangeable the two isomers are, i.e. to what extent kinetics governs the equilibrium. To answer this question the energy barrier between them has been evaluated through DFT/3-21G*. Although the transition structure (TS) between A and B could be supposed to go through a five-coordinate Cr species, it seems more likely that it goes through a rotation about the C–C bond. Such a rotation is expected to proceed more easily as indicated by the long C(1)–C(2) distance (1.493(8) Å), which has mainly a character of single bond. An amount of 15.1 kcal mol^{-1} is required in order to reach the TS from conformer A. This rather high value for the energy barrier arises from the fact that conjugation is decreased when going from conformers A and B to the TS, because in the latter species the carbonylic group is no longer coplanar with the ring. On the whole, the interchange from A to B appears to be somewhat unfavourable kinetically, yet feasible thermodynamically; as regards the gas phase, theoretical results based on relative energies are not in contradiction with a possible coexistence of both conformers. Similar conclusions are drawn when solvent effects are included; single-point calculations on the geometry optimized at RHF level have led to an energy difference of just 0.61 kcal mol^{-1}, favouring conformer A. In solution, we expect an equilibrium between these two conformers, since there is no kinetic or thermodynamic reason which justifies a different conclusion. Therefore, the presence of only conformer A in the X-ray analysis is attributed to crystal effects.

4.2. Electronic analysis

To obtain a further insight into the nature and chemical interactions of compound **1**, topological analyses of the electron density distribution (Fig. 5(a)) and the Laplacian of the electron density (Fig. 5(b)) for conformer A have been built (RHF/3-21G*). The electron density contour is a physical observable and, therefore, it is directly comparable with experimental X-ray diffraction results. The Bader electronic analysis [57] has become a widespread technique to analyze the different characteristics of interactions between atoms in molecules. This kind of analysis is based on the study of the topological properties of electron density distributions and its derivatives (gradient vector and Laplacian).

In the isodensity contour of Fig. 5(a), nuclei are clearly shown by the accumulation of concentric lines around them. Likewise, the so-called bond critical points (BCP) can be envisaged. These are points that exhibit a minimum value of electron density in a path connecting two nuclei but have an electron density maximum in a direction orthogonal to this path. The chemically most interesting BCP of our species are collected in Table 6. Results from this table can be analyzed as follows. (i) The distance of the BCP from the oxygen atoms (r_c) give us a first qualitative idea of the size of the electronic domain for these oxygen atoms. The ordering

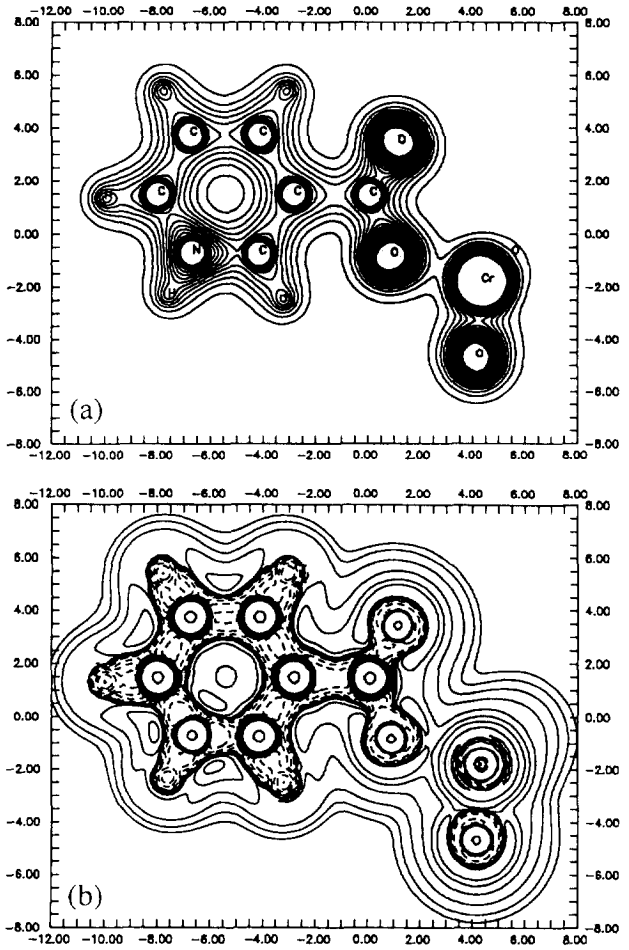

Fig. 5. (a) Topological electron density contour. (b) Laplacian of the electron density map. (Both for conformer A.)

obtained from the r_c values (O(T), 0.74 < O(5), 0.80 < O(4), 0.91 as the average value) is in agreement with that obtained from the Mulliken atomic charge population of the oxygen atoms (O(T), −0.51 < O(5), −0.74 < O(4), −0.88), thus showing that the larger the electronic boundary of oxygens in this molecule, the more negative the atomic charge population is. (ii) Values of the electron density at the BCP ($\rho(r_c)$) allow us to obtain a first approximation on the bond strength. Comparisons can only be made between the same couple of atoms in different atomic environments. They are usually well correlated with bond lengths too. Thus, from these assumptions, it is found, as before, that Cr–O(T) are stronger than Cr–O(4). (iii) The Laplacian of the electron density ($\nabla^2\rho(r)$) provides also important information on the nature of the chemical interaction between atoms. A representation of $\nabla^2\rho(r)$ exhibits spherical nodes in an atom (values of the radius for which $\nabla^2\rho(r) = 0$) and their number is found to be related to its shell structure. Negative values denote regions where electron density is locally concentrated while positive values show regions where electron density is depleted. The initial sphericity of each principal quantum shell in an isolated atom becomes distorted due to the presence of the other constituent atoms in a molecule (see Fig. 5(b)).

A detailed analysis of the set of r, $\rho(r)$, $\nabla^2\rho(r)$ and $|\lambda_1|/\lambda_3$ values reported in Table 6 allows to establish the nature of the atomic interactions in the studied species. Three kinds of interactions can be clearly differentiated. (1) Closed-shell interactions: the first two bonds between chromium and oxygen atoms (Cr(1)–O(T) and Cr(1)–O(4)) belong to this class, although $\rho(r)$ values are larger than it is usually expected for this type of interactions. Location of the BCP is approximately midway between the two atoms, $\nabla^2\rho(r)$ has a significant positive value and $|\lambda_1|/\lambda_3$ has a value of ca. 0.2. This fact can be even more emphasized by looking at Fig. 5(b), where it can be observed that the spherical nature of Cr(1), O(T) and O(4) (facing the chromium atom) atoms is mostly preserved. (2) Intermediate interactions: to this class belong the three next bonds collected in Table 6. C–O and C–N bonds are characteristic of this type of interaction. In these cases distance of the BCP from O or N is practically twice that from C, there is a considerable amount of electron density at the BCP, $\nabla^2\rho(r)$ has a positive value and $|\lambda_1|/\lambda_3$ is lower than one. (3) Shared interactions: to be compared with the other two types of interactions a typical set of values for this kind of interaction (in this case a C–C bond) has also been added at the end of Table 6. From our analysis, compound **1** can be described as a pyridinium derived organic ligand and a chromate as part of the same molecule, interacting as an ion pair complex. This conclusion is confirmed by means of a Mulliken charge distribution anal-

Table 6
Location and characterization of bond critical points (BCP) for compound **1**, where r is the location of the BCP (in Å), $\rho(r)$ is the electron density at the BCP (in e au^{-3}), and $\nabla^2\rho(r)$ is the Laplacian of the electron density at the BCP (in e au^{-5}). The resulting eigenvalues of the Hessian matrix at the BCP (λ_1, λ_2, λ_3) are also given

Bond	r [a]	$\rho(r)$	$\nabla^2\rho(r)$	λ_1	λ_2	λ_3	$\lvert\lambda_1\rvert/\lambda_3$
Cr(1)–O(T)	0.790–0.739	0.306	1.549	−0.638	−0.593	2.780	0.230
Cr(1)–O(4)	0.939–0.961	0.110	0.517	−0.174	−0.165	0.856	0.203
C(1)–O(4)	0.426–0.855	0.332	0.012	−0.802	−0.741	1.555	0.516
C(1)–O(5)	0.398–0.796	0.407	0.706	−1.097	−1.065	2.868	0.382
C(3)–N(1)	0.434–0.904	0.301	0.114	−0.638	−0.527	1.279	0.499
C(1)–C(2)	0.687–0.841	0.232	−0.581	−0.439	−0.418	0.276	1.591

[a] Distance from the first atom–distance from the second atom.

ysis, which shows that the calculated charge separation in compound **1** is $[HNic]^{-0.4}[CrO_3]^{+0.4}$.

4.3. Infrared spectra

Experimentally, infrared spectra of compounds **1** (Fig. 6) and **3** show bands at 3200 cm^{-1} for the first compound and 3127–3076 cm^{-1} for the second, characteristic of symmetrical N–H stretching vibrations of pyridine ring in non-hydrogen bonded pyridinium salts [58]. Bands observed at 1660, 1530, 1327, 1301 and 1250 cm^{-1} for 3-$HNicCrO_3$ and 1665, 1592, 1343 and 1299 cm^{-1} for 4-$HNicCrO_3$, all characteristic of pyridinium ion [58] confirm the previous assignation. These results indicate that the proton (counter-ion) is on the pyridinic nitrogen for the compounds *n*-$HNicCrO_3$ ($n=3,4$). The $C(1)O(5)O(4)^-$ group coordinated to the metal also absorbs at 1660 cm^{-1} for compound **1** and 1665 cm^{-1} for **3**.

The infrared spectrum of **2** presents bands at 3100–3036 cm^{-1} corresponding to N–H stretching vibrations of pyridinium and 1597, 1496 and 1347 cm^{-1}, characteristic of pyridine-4-carboxylic acid. Moreover, one broad band at 2700–2400 cm^{-1} corresponding to ν(OH) of the COOH group is observed. In this compound there is one band at 1713 cm^{-1} assigned to unionized and uncoordinated COO stretching vibration [59]. These results are both in accordance with the existence of the pyridinium-4-carboxylic acid which acts as the counter-ion in compound **2**.

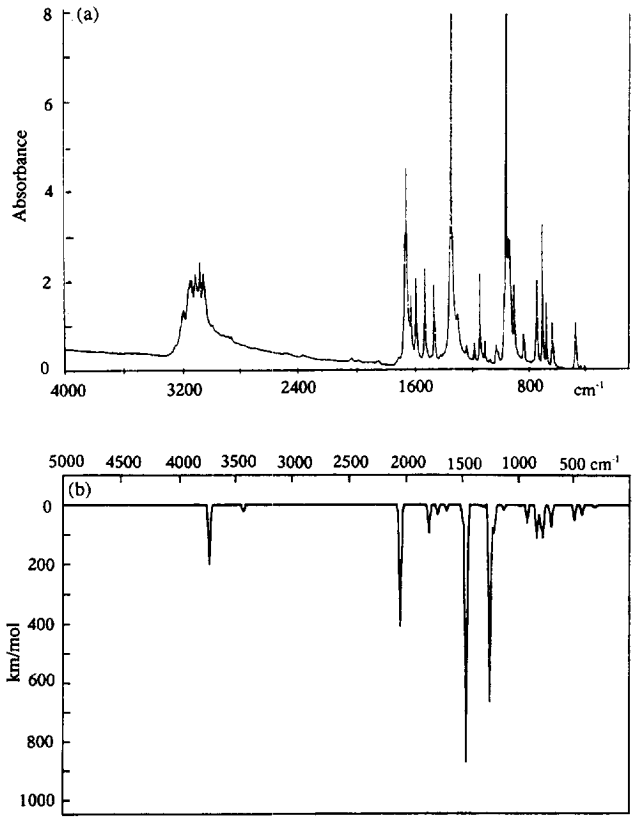

Fig. 6. IR spectra for 3-$HNicCrO_3$ compound: (a) experimentally recorded shape; (b) computationally calculated shape (conformer A).

The Cr–O(T) symmetric and antisymmetric stretching vibrations are found as strong bands at 976, 959 and 906 cm^{-1} for the compound **1**, 955 and 937 cm^{-1} for the compound **2** and 965, 957, 946 and 903 cm^{-1} for the compound **3**.

In theory, 48 normal modes are expected for a 18-atom molecule such as 3-$HNicCrO_3$. However, only the most significant peaks that appear on the range 600–3800 cm^{-1} will be analyzed. As shown in Fig. 6, the shape of the computationally simulated IR spectrum is in excellent agreement with experiment. Thus, the main features are well reproduced, not only regarding to spacings but also concerning relative intensities.

As one can see, computed frequencies appear systematically above experimental peaks. It is well known that all-electron Pople's basis sets such as 3-21G*, used at a SCF level, overestimate frequencies, and that a scaling factor of 0.8–0.9 usually needs to be applied [60,61]. Taking this fact into account, the aforementioned displacement of peak positions may be scaled in order to properly elucidate and confirm the experimental characterization. For instance, the computed N(1)–H stretching vibration at 3714.8 cm^{-1} corresponds (after applying the correction factor) to that reported at 3200 cm^{-1}, confirming the formation of a pyridinium salt (as the final product) as a result of H^+ migration towards N in the last step of the mechanism. Unscaled symmetric and antisymmetric Cr(1)–O(4) stretchings are found at 1236.2 and 1238.9 cm^{-1}, respectively, whereas the Cr–O(T) symmetric stretching appears at 1209.3 cm^{-1}, all being in fair agreement with experiment when multiplied by the correction factor. Similar values were found in a previous work [44] on $Cr_2O_7^{2-}$ species; in particular, a value of 1174 cm^{-1} was reported for ν_{as}(Cr–O(T)), using a 3-21G basis set. The calculated peak at 2038.78 cm^{-1} should be assigned (after being corrected) to the C=O stretching vibration of the COO^- group, which absorbs at 1660 cm^{-1}. We can also assign the stretching vibration of the O(4)–Cr(1) bond. It is computed at 686.0 cm^{-1}, corresponding to a corrected value of ca. 585 cm^{-1}.

Analyzing the aromatic region, bending vibrations of the ring are found at 779.7 and 762.9 cm^{-1} (in- and out-of-plane, respectively). A close peak at 820.2 cm^{-1} is due to a superposition of N(1)–H and C–H bendings. Comparison with the calculated spectrum for $HCrO_4^-$ species emerges as an interesting point, because it allows for clearly visualizing the contribution of the chromate fragment in 3-$HNicCrO_3$ compound, without any interference due to ring absorptions, i.e., it serves to confirm previous assignments. Thus, for instance, Cr–O symmetric and antisymmetric stretching vibrations for the $HCrO_4^-$ species appear in the region 1188–1226 cm^{-1}, whereas for compound **1** are located essentially in the same range (1209–1239 cm^{-1}), pyridinium ring effects being responsible for the very slight displacement of peaks.

4.4. Electronic spectra

From experimental data, the three compounds studied in this paper exhibit the same bands in the electronic spectra in

solid state. For a first interpretation of the spectra, we can make use of the orbital energies for CrO_4^{2-} anion calculated using the X_α-scattered wave method [29], and also our recently reported transition values for dichromate [44]. In compound **1**, the observed band at 360 nm (3.44 eV) corresponds to the parent transition $t_1^6 \rightarrow t_1^5e^1$ in the CrO_4^{2-} model (calculated: 3.3 eV [29]), and the band at 273 nm (4.54 eV) corresponds to the parent transition $t_1^6 \rightarrow t_1^5t_2^1$ (calculated: 4.23 eV). A weak band near 450 nm is probably electric dipole forbidden [62]. The electronic spectra also show one band at 216 nm corresponding to carbonyl chromophore ($n \rightarrow \sigma^*$) and one band at 255 nm characteristic of the pyridinium ring [63].

The simulation of the UV–vis spectrum of 3-$HNicCrO_3$ species through classical ab initio single-excitation calculations requires a computational effort that is beyond the currently available computers. A reasonable alternative would indeed consist of performing the study for the smaller $HCrO_4^-$ anion instead of the 18-atom molecule. Nevertheless, density functional theory offers an elegant way of solving the former question at a cost cheaper than the usual single-excitation configuration interaction theory (CIS) [64]. Thus, using the sum method [46], several transitions involving the higher occupied and the lower unoccupied molecular orbitals have been computed for compound **1** (BP/STO double-ζ basis set plus polarization functions). The most interesting feature emerges from the HOMO–LUMO transition because, according to our calculations, it demands an energy of 3.38 eV, which corresponds to a wavelength of 367 nm, close to the experimentally observed bands at 351 and 444 nm in the electronic spectrum and, moreover, which accounts for the intense orange-yellowish colour of these compounds. As regards to molecular orbitals, the nature of the transition can be classified as a ligand-to-metal charge-transfer (LMCT) transition, where an electron is promoted from a lone pair of oxygens O(T) to the lowest-lying empty *d* antibonding orbital.

5. Concluding remarks

Three compounds belonging to the pyridine–chromium (VI) family of oxidizing agents have been synthesized at room temperature in an aqueous solution, and have been characterized by chemical analysis, ^1H NMR, IR and UV–vis spectra, and X-ray diffraction. Structural experimental data for pyridinium-3-carboxylate trioxochromate (VI) obtained by X-ray diffraction have been complemented by a theoretical study. A new crystal phase (triclinic), different from that reported previously [19] (monoclinic), has been reported here using other synthetic conditions. Two similar compounds based on the isonicotinic acid have been also reported for the first time. From the point of view of reactivity, more than one step appears to be needed in order to reach the products, the $HCrO_4^-$ species being thought to act as a key intermediate. This species has been taken as reference to study the spectroscopic features of these chromium compounds.

As far as compound 3-$HNicCrO_3$ is concerned, two different conformers are theoretically possible. Computed relative energies and activation barriers suggest that, in the gas phase and in aqueous solution, coexistence of the two conformers is feasible, so both of them should be expected to be found. Intermolecular forces leading packing, together with other related factors can account for a unique structure having been reported experimentally from X-ray diffraction studies of the solid product. By means of an electronic analysis of the species studied, a further insight in their theoretical characterization has been obtained. Not only the size of electronic domains and the strength of bonds according to atomic environments have been analyzed, but also the nature of chemical interactions has been clarified. Infrared spectra have been recorded and analyzed for the species under study, assignments being in fair agreement with calculated predictions. Results indicate that for compounds *n*-$HNicCrO_3$ ($n = 3,4$) the counter-ion is located on the nitrogen atom. Finally, regarding UV–vis spectra, it has been noted that predicted colour considerations are consistent with experimental evidence.

6. Supplementary material

Tables of complete crystallographic data, final atomic coordinates and anisotropic thermal parameters, hydrogen atom parameters, torsion angles, intermolecular contacts, and least-squares planes. Ordering information is given on any current masthead page.

Acknowledgements

We acknowledge the partial financial support of the Spanish "Dirección General de Investigación Científica y Técnica" (Project PB92-0333). One of us (M.T.) gratefully acknowledges the financial support provided by the "Comissionat per a Universitats i Recerca de la Generalitat de Catalunya" through a Graduate Fellowship. We also thank the Spanish "Comisión Interministerial de Ciencia y Tecnología" for a generous gift of computer time on the CRAY computer at CIEMAT Madrid.

References

[1] E.J. Corey and G. Schmidt, *Tetrahedron Lett.*, *5* (1979) 399.
[2] H.B. Davis, R.M. Sheets, W.W. Paudler and G.L. Gard, *Heterocycles*, *22* (1984) 2029.
[3] K. Balasubramanian and V. Prathibe, *Ind. J. Chem. B*, *25* (1986) 326.
[4] J. Muzart, *Chem. Rev.*, *92* (1992) 113.
[5] P. Martin-Zarza, P. Gili, F.V. Rodriguez-Romero, C. Ruiz-Perez and X. Solans, *Polyhedron*, *14* (1995) 2907.

[6] P.A. Lorenzo Luis, P. Martin-Zarza, P. Gili, J.M. Arrieta, G. Germain and L. Dupont, *Eur. J. Solid. State Inorg. Chem., 32* (1995) 353.
[7] J. Pérez-Benito and C. Arias, *An. Quim., 89* (1993) 636.
[8] A.S. Standeven and K.E. Wetterhahn, *J. Am. Coll. Toxicol., 8* (1989) 1275.
[9] D. Burrows (ed.), *Chromium: Metabolism and Toxicity*, CRC Press, Boca Raton, FL, 1983.
[10] A.G. Levis and V. Bianchini, in S. Langard (ed.), *Biological and Environmental Aspects of Chromium*, Elsevier, Amsterdam, 1982, pp. 171–208.
[11] R.B. Hays, in S. Langard (ed.), *Biological and Environmental Aspects of Chromium*, Elsevier, Amsterdam, 1982, pp. 221–247.
[12] S. Brown and Y. Kadamma, *Toxicology of Metals Clinical and Experimental Research*, Ellis Horwood, New York, 1987, p. 129.
[13] M. Cieslak-Golonka and M. Raczko, *Polyhedron, 11* (1992) 2549.
[14] S.L. Brauer and K.E. Wetterhahn, *J. Am. Chem. Soc., 113* (1991) 3001.
[15] P.A. Meloni and R.S. Czernuszewicz, *Vibrational Spectroscopy, 5* (1993) 205.
[16] P.H. Connett and K.E. Wetterhahn, *J. Am. Chem. Soc., 107* (1985) 4282.
[17] R.N. Bose, S. Moghaddas and E. Gelerinter, *Inorg. Chem., 31* (1992) 1987.
[18] R.K. Murray, D.K. Granner, P.A. Mayes and V.W. Rodwell, *Harper's Biochemistry*, Prentice Hall, Englewood Cliffs, NJ, 1993.
[19] C. López, A. González, F.P. Cossío and C. Palomo, *Synth. Commun., 15* (1985) 1197.
[20] J.K.T. Matikainen, S.A.A. Kaltia, T.A. Hase, M.R. Sundberg and R. Kivekäs, *J. Chem. Res. (S), 5* (1990) 150; *J. Chem. Res. (M), 5* (1990) 1117.
[21] D.R. Salahub and M.C. Zerner (eds.), *The Challenge of d and f Electrons: Theory and Computations, ACS Symp. Ser. 394*, American Chemical Society, Washington, DC, 1989.
[22] A. Veillard (ed.), *Quantum Chemistry: The Challenge of Transition Metal and Coordination Chemistry*, Kluwer, Dordrecht, Netherlands, 1986.
[23] R. Arratia-Pérez and C.Y. Yang, *J. Chem. Phys., 83* (1985) 4005.
[24] L.A. Barnes, M. Rosi and C.W. Bauschlicher, Jr., *J. Chem. Phys., 94* (1991) 2031.
[25] L.A. Barnes, B. Liu and R. Lindh, *J. Chem. Phys., 98* (1993) 3978.
[26] J. Li, G. Schreckenbach and T. Ziegler, *J. Phys. Chem., 98* (1994) 4838.
[27] A.W. Ehlers and G. Frenking, *J. Am. Chem. Soc., 116* (1994) 1514.
[28] M. Aarnst, D.J. Stufkens, M. Solà and E.J. Baerends, *Organometallics*, in press.
[29] R.M. Miller, D.S. Tinti and D.A. Case, *Inorg. Chem., 28* (1989) 2738.
[30] T. Ziegler and J. Li, *Organometallics, 14* (1995) 214.
[31] M. Torrent, P. Gili, M. Duran and M. Solà, *J. Chem. Phys., 104* (1996) 9499.
[32] M.G. Cory and M.C. Zerner, *Chem. Rev., 91* (1991) 813.
[33] A. Veillard, *Chem. Rev., 91* (1991) 743.
[34] G.M. Sheldrick, *SHEXTL-PLUS*, Release 4.21, Siemens Analytical X-ray Instruments, Madison, WI, 1991.
[35] *International Tables for X-Ray Crystalography*, Vol. IV, Kynoch Press, Birmigham, UK, (present distributor: Kluwer, Dordrecht, Netherlands), 1974.
[36] K. Yvon, W. Jeitschko and E. Parthe, *J. Appl. Crystallogr., 10* (1977) 73.
[37] E. Pretsch, T. Clerc, J. Seibl and W. Simon, *Tabellen zur Strukturaufklärung organischer Verbindungen mit spektroskopischen Metoden*, Springer, Berlin, 1976.
[38] A.D. Becke, *Phys. Rev. A, 38* (1988) 3098.
[39] J.P. Perdew, *Phys. Rev. B, 33* (1986) 8822.
[40] F. Maseras, M. Duran, A. Lledós and J. Bertrán, *J. Am. Chem. Soc., 28* (1991) 2984.
[41] A. Lledós, M. Duran, Y. Jean and F. Volatron, *Inorg. Chem., 40* (1991) 511.
[42] V. Branchadell and A. Dedieu, *New J. Chem., 12* (1988) 443.
[43] (a) J.S. Binkley, J.A. Pople and W.J. Hehre, *J. Am. Chem. Soc., 102* (1980) 939; (b) M.S. Gordon, J.S Binkley, J.A. Pople, W.J. Pietro and W.J. Hehre, *J. Am. Chem. Soc., 104* (1982) 2797; (c) W.J. Pietro, M.M. Francl, W.J. Hehre, D.J. Defrees, J.A. Pople and J.S. Binkley, *J. Am. Chem. Soc., 104* (1982) 5039.
[44] J. Mestres, M. Duran, P. Martín-Zarza, E. Medina de la Rosa and P. Gili, *Inorg. Chem., 32* (1993) 4708.
[45] H.B. Schlegel, *J. Comput. Chem., 3* (1982) 214.
[46] T. Ziegler, *Chem. Rev., 91* (1991) 651.
[47] M.J. Frisch, G.W. Trucks, M. Head-Gordon, P.M.W. Gill, M.W. Wong, J.B. Foresman, B.G. Johnson, H.B. Schlegel, M.A. Robb, E.S. Replogle, R. Gomperts, J.L. Andres, K. Raghavachari, J.S. Binkley, C. Gonzalez, R.L. Martin, D.J. Fox, D.J. Defrees, J. Baker, J.J.P. Stewart and J.A. Pople, *Gaussian 92*, Revision A, Gaussian, Pittsburgh, PA, 1992.
[48] *Amsterdam Density Functional*, Vrije Universiteit, De Boelelaan 1083, 1081 HV Amsterdam, Netherlands, 1993.
[49] E.J. Baerends, D.E. Ellis and P.E. Ros, *Chem. Phys., 2* (1973) 41.
[50] (a) S. Miertuš and J. Tomasi, *Chem. Phys., 65* (1982) 239; (b) S. Miertuš, E. Scrocco and J. Tomasi, *Chem. Phys., 55* (1981) 117.
[51] *Electra*, J. Mestres, IQC, Girona CAT, 1994.
[52] W. Mazurek, P.J. Nichols and B.O. West, *Polyhedron, 10* (1991) 753.
[53] F. Brito, J. Ascanio, S. Mateo, C. Hernández, L. Araujo, P. Gili, P. Martín-Zarza, S. Domínguez and A. Mederos, submitted for publication.
[54] R. Duval and C. Duval, *Nouveau Traité de Chimie Minérale, 14*, Masson, Paris, 1959, p. 537.
[55] M.R. Pressprich, R.D. Willet, R.D. Poshusta, S.C. Saunders, H.B. Davis and G.L. Gard, *Inorg. Chem., 27* (1988) 260.
[56] C. Sosa, J. Andzelm, B.C. Elkin, E. Wimmer, K.D. Dobbs and D.A. Dixon, *J. Phys. Chem., 96* (1992) 6630.
[57] (a) R.F.W. Bader, *Atoms in Molecules. A Quantum Theory*, Oxford University Press, Oxford, UK, 1990; (b) R.F.W. Bader, *Chem. Rev., 91* (1991) 893.
[58] N.S. Gill, R.H. Nuttall, D.E. Scaife and D.W.A. Sharp, *J. Inorg. Nucl. Chem., 18* (1961) 79.
[59] K. Nakamoto, *Infrared and Raman Spectra of Inorganic and Coordination Compounds*, Wiley, New York, 4th edn., 1986.
[60] J.B. Foresman and E. Frisch, *Exploring Chemistry with Electronic Structure Methods: A Guide to Using Gaussian*, Gaussian Pittsburgh, PA, 1st edn., 1993.
[61] W.J. Hehre, L. Radom, P.R. Schleyer and J.A. Pople, *Ab Initio Molecular Orbital Theory*, Wiley, New York, 1986.
[62] A.B.P. Lever, *Inorganic Electronic Spectroscopy*, Elsevier, Amsterdam, 2nd edn., 1984.
[63] P. Gili, *Revue Chim. Miner., 24* (1984) 171.
[64] J.B. Foresman, M. Head-Gordon and J.A. Pople, *J. Phys. Chem., 96* (1992) 135.